Nanoscale analysis of a $SrTiO_3/La_{2/3}Sr_{1/3}MnO_3$ interface

F. Pailloux,[1] D. Imhoff,[2] T. Sikora,[2] A. Barthélémy,[1] J.-L. Maurice,[1] J.-P. Contour,[1] C. Colliex,[2,3] and A. Fert[1,*]
[1]*Unité mixte de Physique CNRS/THALES, Domaine de Corbeville, 91404 Orsay Cedex, France and Université Paris-Sud, 91405 Orsay Cedex, France*
[2]*Laboratoire de Physique des Solides, UMR CNRS 8502, Bâtiment 510, Université Paris Sud, 91405 Orsay, France*
[3]*Laboratoire Aimé Cotton, UPR CNRS 3321, Bâtiment 505, Université Paris Sud, 91405 Orsay, France*
(Received 9 October 2001; published 8 July 2002)

The aim of the present work is an atomic scale characterization of the $SrTiO_3/La_{2/3}Sr_{1/3}MnO_3$ interface involved in $Co/SrTiO_3/La_{2/3}Sr_{1/3}MnO_3$ tunnel junctions. Our high-resolution transmission electron microscopy experiments show the quality of the pseudo-morphic growth of $La_{2/3}Sr_{1/3}MnO_3$ (LSMO) and $SrTiO_3$ (STO), but do not allow us to determine the termination of LSMO. On the other hand, we have carried out an energy-loss near-edge structure study of the Mn_{2p} and O_{1s} edges. The main result is that the valence of Mn keeps its intrinsic value of the bulk material till the last MnO_2 layers at the interface, which is consistent with the observation of magnetoresistance up to practically the Curie temperature of bulk LSMO in our junctions. These results suggest a $La_{2/3}Sr_{1/3}O$ termination of LSMO.

DOI: 10.1103/PhysRevB.66.014417 PACS number(s): 75.45.+j, 82.80.Pv, 68.37.Lp, 85.30.Mn

I. INTRODUCTION

Half-metallic ferromagnets are, in principle, ideal materials for spin electronics since they are expected to present a complete spin polarization of their electron states at the Fermi level. It is true that record magnetoresistances (MR's) have been obtained in tunnel junctions with electrodes made of half-metallic manganites like $La_{2/3}Sr_{1/3}MnO_3$ (LSMO) or $La_{2/3}Ca_{1/3}MnO_3$ (LCMO), but, disappointingly, these huge MR effects decrease as a function of temperature much more rapidly than it could be expected from the value of the Curie temperature (T_c) in bulk materials.[1–4] What is actually important in tunnel junctions and other heterostructures is the spin polarization not in the bulk half-metallic ferromagnet but at its interfaces with other materials. An interesting correlation has been found between the temperature dependence of the junction resistance and the drop of the magnetoresistance with temperature in LSMO/STO/LSMO tunnel junctions (STO is $SrTiO_3$).[2] As the temperature increases from 4.2 K, the junction resistance increases, as normally expected from the decrease of the carrier density in LSMO when the magnetic disorder increases. A resistance maximum, corresponding to a carrier density minimum, is expected at the Curie temperature of LSMO (also at the metal-insulator transition), but, surprisingly, the junction resistance maximum is found at about 200 K, well below the Curie temperature of bulk LSMO (around 350 K). This temperature has been identified to the ''effective'' Curie temperature[5] at the LSMO/STO interface. Quite consistently, the MR vanishes at this temperature (inset of Fig. 1). Similar collapses of the MR at temperatures well below T_c^{bulk} (generally below $T_c^{bulk}/2$) have been found in other tunnel junctions with LSMO or LCMO electrodes,[1,2,4] and it is tempting to conclude that this strong reduction of the ''effective'' Curie temperature at interfaces is an unavoidable intrinsic property of heterostructures with half-metallic oxides.

However, this conclusion of unavoidable large reduction of the ''effective'' Curie temperature at interfaces is in contradiction with more recent experiments. The tunnel magnetoresistance (TMR) vanishes only at 270 K in some junctions studied by Noh *et al.*[3] Moreover TMR is still observed at room temperature in Co/STO/LSMO junctions, and vanishes only at 320–330 K, practically the Curie temperature of bulk LSMO (around 350 K). We refer to the work in our laboratory on Co/STO/LSMO tunnel junctions[6,7] in which the STO/LSMO basis is deposited by laser ablation in the same conditions as for the LSMO/STO/LSMO junctions[2] of the discussion above, before depositing a Co layer on STO. The temperature dependence of the MR in a Co/STO/LSMO junction[7] is shown in Fig. 1: at low temperature the MR (50%) is smaller than in junctions with two LSMO electrodes (as expected from the moderate polarization of Co in comparison with LSMO) but, in contrast, the MR decreases more slowly with temperature and vanishes only at about 330 K, that is practically at T_c^{bulk}. Consistently the maximum of tunnel resistance is also close to T_c^{bulk}. This absence of a T_c reduction when only a ''bottom'' STO/LSMO interface is involved indicates that the ''effective'' Curie temperature of this ''bottom'' interface is close to T_c^{bulk}, and suggests that, in the LSMO/STO/LSMO junctions prepared in the same conditions,[2] only the top LSMO/STO interface presents a strongly reduced T_c and is responsible for the rapid MR drop with temperature.

The problem of the structure at LSMO/STO (or LCMO/STO) interfaces and the influence of this structure on the physical properties were already discussed in several publications, for example in Refs. 7 and 8. Strain, presence of defects, roughness, departures from stoichiometry can affect the physical properties and, in the case of superlattices, Izumi *et al.*[8] in particular put forward the influence of the termination of the manganite at the interface. As will be discussed in more detail in Sec. III and in the following, the most probable terminations at a (001) interface are those represented in Fig. 2. In a type-I termination [Fig. 2(a)], the LSMO layer is terminated by a $La_{2/3}Sr_{1/3}O$ atomic layer, so that the environment of the Mn atoms in the adjacent MnO_2 layer is approximately the same as in bulk LSMO. Such a

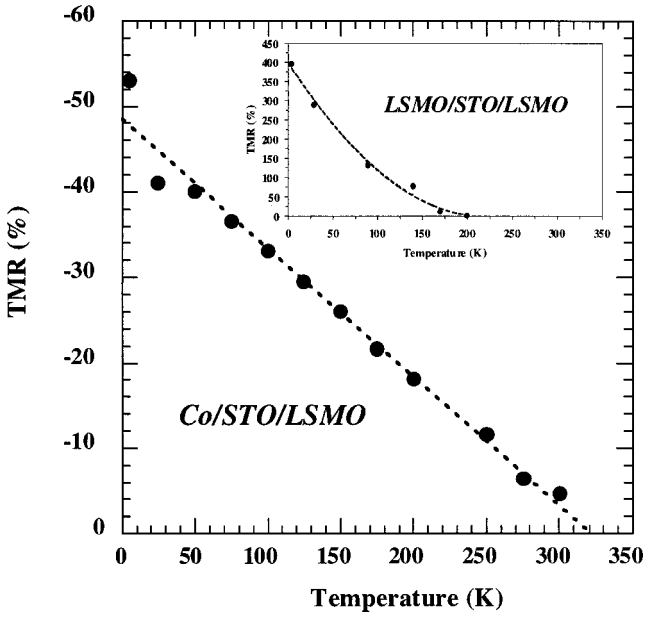

FIG. 1. Temperature dependence of the TMR in a Co/STO/LSMO junction (Ref. 6). Inset: temperature dependence of the TMR in a LSMO/STO/LSMO junction in which the STO/LSMO bottom bilayer has been prepared in the same conditions as for the Co/STO/LSMO junction.

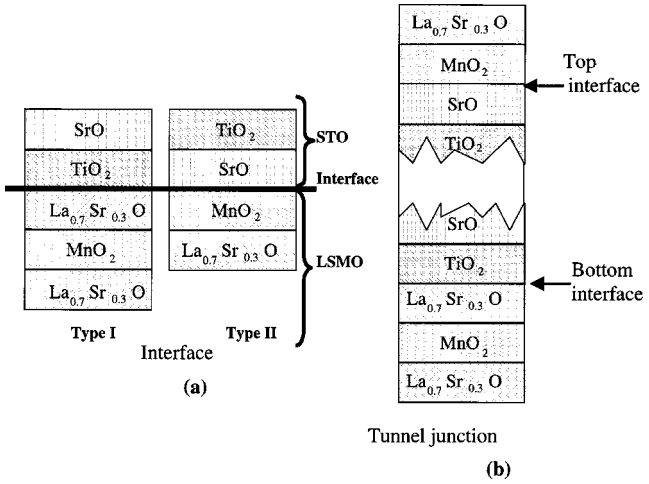

FIG. 2. (a) Type-I and -II terminations at a LSMO/STO interface. (b) Possible scenario for a LSMO/STO/LSMO tunnel junction explaining that the effective Curie temperature is reduced. In the type-I structure of the bottom interface, the last MnO_2 layer of LSMO is ''protected'' by a $La_{2/3}Sr_{1/3}O$ atomic plane and has the same environment than in the bulk. The T_C of the bottom electrode is then that of the bulk. In contrast, the top electrode has type-II structure, the MnO_2 layer is in direct contact with the barrier, leading to different proportion of La^{3+} and Sr^{2+} than in the bulk resulting in a reduced Curie temperature for this interface and then a reduced T_C for the tunnel junction. This scenario would explain that the TMR remains above room temperature when only the bottom interface is involved [Co/STO/LSMO junctions (Ref. 7)], but decreases much more rapidly in a LSMO/STO/LSMO tunnel junction where both interfaces are present.

''protected'' MnO_2 layer is expected to be weakly influenced by the proximity of STO. With a termination of type II [Fig. 2(b)], the interface MnO_2 layer is between La_0Sr_1O (SrO) and $La_{2/3}Sr_{1/3}O$ layers. As one knows the extreme sensitivity of the Curie temperature of LSMO to the proportion of La^{3+} and Sr^{2+}, one can predict that a configuration of type II should lead to a reduction of T_c in the region of the interface. A plausible explanation of the very different effective T_c, observed in junctions with a single or two LSMO electrodes, could therefore be a picture with different terminations, type I for the bottom interface of the junctions, and type II for the top interface of the LSMO/STO/LSMO junctions. It is, however, clear that other features of the interface structure could also play a significant role.

To obtain a better insight into the structure of the interfaces in LSMO/STO/LSMO and Co/STO/LSMO tunnel junctions, and to understand more clearly the main features affecting the spin polarization properties, we have carried out an extensive investigation of the structure of the STO/LSMO interface (this is a ''bottom interface'') in one of our Co/STO/LSMO junctions by high-resolution transmission electron microscopy (HRTEM) and scanning transmission electron microscopy–electron-energy-loss spectroscopy (STEM-EELS). In Sec. II we describe the experimental and simulation methods we used for the structural and chemical characterization of the interfaces. In Sec. III A we describe data concerning the interface structure obtained by HRTEM and in Secs. III B and III C we present and discuss the results we obtain from STEM-EELS on the environment and valence of the Mn ions at the interfaces. Our results for the ''bottom'' STO/LSMO interface confirm that the intermediate valence of Mn in bulk LSMO is preserved due probably to a termination similar to type I in Fig. 2. This is consistent with the very weak reduction of T_c observed in tunnel junctions where only the first STO/LSMO interface is present (such as in Co/STO/LSMO junctions[7]). This is a first step before a similar study of a ''top'' LSMO/STO interface to understand the difference in the termination or structure at the origin of the more strongly reduced T_c of LSMO/STO/LSMO tunnel junctions where the ''top'' LSMO/STO interface is also involved.

II. EXPERIMENTAL METHODS

A. Thin foil preparation

We have investigated the microstructure of the STO/LSMO interface using HRTEM experiments combined with image simulations, and the chemical bonding at this interface using EELS measurements in a STEM microscope. These two techniques require thin foils of constant thickness over the studied areas, sufficiently thin to preserve the intrinsic high-resolution capabilities of the two methods. Furthermore, the specimens must be thinned so that the investigated interface is oriented parallel to the electron beam, i.e., perpendicular to the specimen surfaces. The accuracy of this alignment must be better than a few degrees in angle which can be compensated by the tilting mechanisms of the specimen stage (during the HRTEM experiments). To achieve this goal, the cross sections have been prepared by mechanical

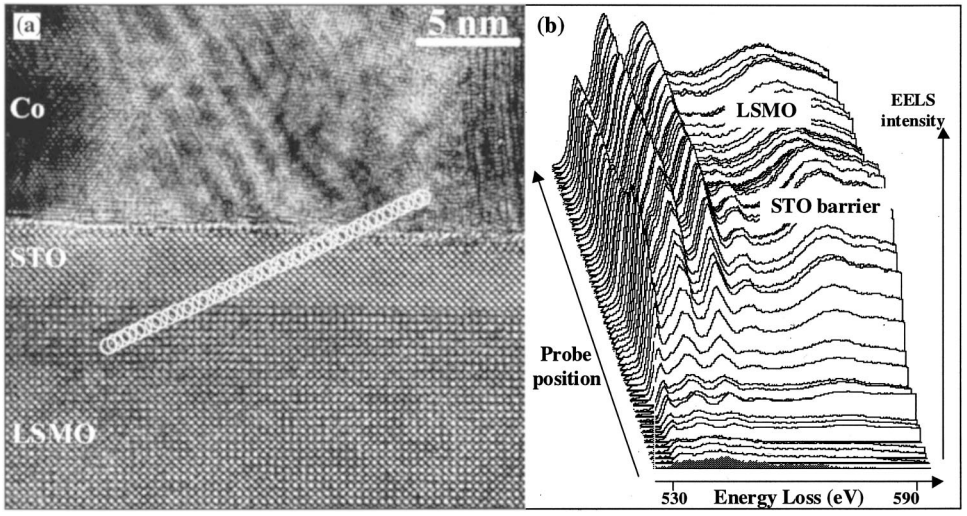

FIG. 3. (a) HRTEM picture of the Co/STO/LSMO tunnel junction showing the epitaxial relationship between the oxide layers. The white circles schematically indicate the probe positions during the EELS experiments (the probe size is about 0.7 nm). (b) three-dimensional EELS image spectrum for the *O*-K edge corresponding to an angle of 20° between the interface planes and the line scan. The probe step between two successive spectra is 0.25 nm and the acquisition time for each spectrum is 200 ms.

thinning using a tripod polisher and diamond coated discs to about 10-μm thickness.[10,11] The thin sections were then argon-ion milled in a PIPS Gatan apparatus. Low-energy ions (2.5 keV) were used to avoid irradiation damage during this step. Small incidence ($\pm 6°$) and sequential rotation were employed to minimize preferential thinning on each side of the interface. These conditions have led to a milling time of approximately two hours to achieve electron transparency over wide areas.

B. HRTEM experiments and contrast simulations

HRTEM images of cross sections were recorded with a TOPCON EM 002B ($C_s = 0.4$ mm) operated at 200 kV (with a point to point resolution of 0.19 nm). Figure 3(a) is an overview of the Co/STO/LSMO tunnel junction. It shows the projection of the pseudocubic unit-cell of the perovskite structure along one of its basic crystallographic axis. Image simulations were carried out with the EMS software package,[12] using the multislice method. The Debye-Waller factors were set to the common value of 5×10^{-3} nm^2 for all atomic species. A standard value (0.6 mrad) of semiconvergence angle for the LaB_6 illuminating system has been used. The aperture diameter corresponding to our experimental condition was 13.79 nm^{-1}, and the defocus spread for our microscope was 8 nm. Absorption coefficients were set to zero during the calculations. The size of simulated images of the perovskite unit cell was 64×64 pixels leading to a sampling of about 6×10^{-3} nm/pixel. The unit cells were cut into two elemental subslices 0.195 nm thick in the beam direction to fulfill the phase object approximation. The same conditions were used during simulation of the STO/LSMO interface contrast. Our multislice calculations were validated by several ways including comparison to Bloch waves simulations performed in the case of pure STO and LSMO.

The optimum conditions to obtain strong contrast for each material and between them can be seen on the thickness-defocus maps of Fig. 4. The best defocus values are between -30 and -40 nm for a sample thickness lying between 17.2 and 18.5 nm. During the experiments, the defocus conditions were estimated from the power spectrum of a thin amorphous area at the edge of the sample close to the working area. Under these conditions, the bright dots observed in STO correspond to the projection of both atomic columns of strontium and TiO. It is worth noting that, for given conditions, these two types of columns give rise to the same kind of contrast (bright or black dots) at the same time. On the other hand, the bright dots seen in the LSMO exclusively correspond to the projection of MnO atomic columns, whereas lanthanum and strontium columns are imaged very weakly.

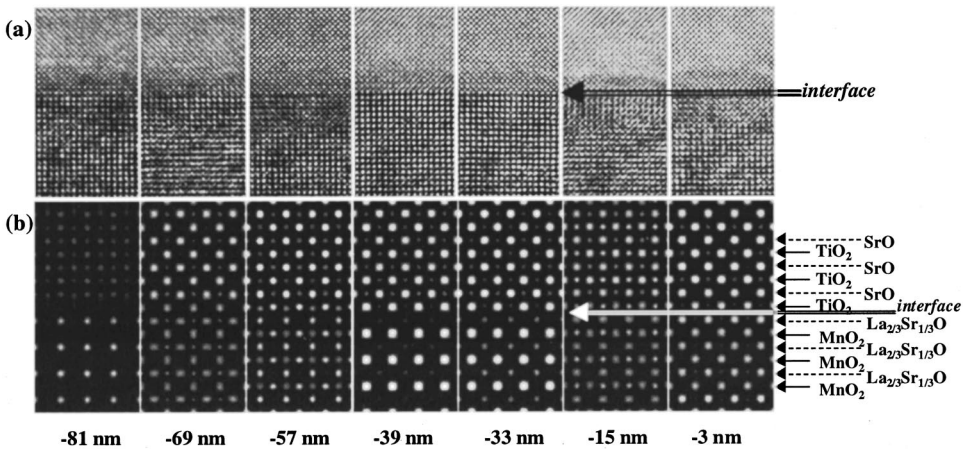

FIG. 4. (a) Experimental through-focus series at a STO/LSMO interface. Optimum contrast is achieved for a defocus value of -33 nm. (b) Multislice contrast simulations of a STO/LSMO interface of type I (sample thickness: 18 nm). Defocus values are indicated at the bottom. For -33 nm, MnO atomic columns (in LSMO) and Sr and TiO atomic columns (in STO) are imaged as bright dots. $La_{2/3}Sr_{1/3}$ atomic columns in LSMO are weakly visible.

C. STEM-EELS

A VG HB 501 dedicated STEM, operated at 100 kV with a field emission gun and equipped with a GATAN parallel EELS spectrometer, modified in the laboratory,[13] is used for the EELS study. The main hardware modification concerns the installation of a CCD camera of 1024×256 pixels with an optical coupling free of optical fibers. The selected areas for EELS correspond to those investigated by HRTEM. Reference spectra for the Mn_{2p} and O_{1s} edges have been collected from standard bulk specimens, such as $La_{0.1}Sr_{0.9}MnO_3$, $La_{2/3}Sr_{1/3}MnO_3$, $LaMnO_3$, and $SrTiO_3$. For the multilayer system, the interface planes are located parallel to the electron beam and controlled from high-angle annular dark field and EELS profiles. Energy dispersions of 0.1, 0.2, and 0.5 eV/ch have been employed. The energy resolution is typically 0.6 eV measured on a zero loss peak. The energy calibration between the different edges is achieved by fixing the zero loss peak and the absorption edges at the same well-defined positions on the detector and by measuring the offset voltage of the spectrometer.

The spectrum-image technique[14] in the line scan mode is used to record one spectrum [Fig. 3(b)] for each probe position along a preselected line scan [Fig. 3(a)]. Many series of 64 to 256 spectra have been acquired at magnifications of 1–5 million, with the scan direction at 15° to 30° across the interface plane, as illustrated in Fig. 3(a). A strong overlap of the probe-sample interaction volume is used between the subsequent spectra, typically 0.3 nm for a beam diameter of 0.7 nm. Therefore, the probe step corresponding to the distance between the beam and the interface plane can be as small as 0.1 nm. For each spectrum, the integration times are typically 50–200 ms for the core-loss energy-loss domain (400–950 eV in the present work). In this energy domain, Ti_{2p} ($\approx$455 eV), O_{1s} ($\approx$530 eV), Mn_{2p} ($\approx$640 eV), Co_{2p} ($\approx$780 eV), and La_{3d} ($\approx$830 eV) edges can be studied. Before any other data treatment, the continuous background is subtracted under the edges by the classic method using a smooth power law. This sophisticated acquisition procedure which produces large amounts of data, is very powerful to detect small variations of energy-loss near-edge structure (ELNES) located in the last atomic planes at the interfaces.

Multivariate statistical analysis (MSA) is the powerful complementary tool of the spectrum-image technique. It increases the signal-to-noise ratio, and identifies and locates the different main sources of information in each series of spectra.[15,16] MSA analyzes the variance and covariance of a multidimensional data set built from each energy channel and probe location. An eigenvector decomposition of the variance-covariance matrix allows one to select the different informations contributing to the overall signal. The analysis of this decomposition determines how far one can use the MSA technique: only for reducing the identified noise (thresholding method) or extended up to quantify ELNES profile (a separate paper is in preparation for a more detailed description of the involved methodologies and limitations). A non-negative least-square (NNLS) fit is also used from various bulk reference spectra.[17]

III. RESULTS AND DISCUSSION

A. Atomic structure: roughness and ordering at the STO/LSMO interface

Growing a perovskite film, along a (001) crystallographic direction, on another perovskite film or substrate, having the same crystallographic orientation, can lead to four different kinds of abrupt (atomically sharp) interfaces. The reason for this lies in the stacking sequence (…-*A*O-BO_2-*A*O-BO_2-…) of this structure.

The first configuration one can consider consists in facing two BO_2-type planes (…-*A*O-$\mathbf{BO_2}$-$\mathbf{B'}O_2$-A'O-…), which in our case corresponds to a MnO_2 plane facing a TiO_2 plane. This configuration is quite unlikely to occur because of the incompatibility of the rutile (TiO_2) structure with the perovskite one.[18] Another possibility is the stacking of two *A*O-type layers face to face (…-BO_2-$\mathbf{AO}$-$\mathbf{A'O}$-$B'O_2$-…). This second configuration may be considered, assuming the formation of a rocksalt layer at the interface, and would lead to a local structure similar to a Ruddlesden-Popper phase, currently observed in off-stoichiometric (*A* excess) perovskite thin films.[19] Thus, the inter-planar distance between the two atomic layers at the interface should be slightly larger ($a_p/\sqrt{2}$) than the half unit-cell of the perovskite ($a_p/2$), leading to a peculiar contrast which is not observed in our experimental pictures.

The other configurations assume the continuation of the perovskite stacking sequence across the interface, either of type I (…-BO_2-$\mathbf{AO}$-$\mathbf{B'}O_2$-A'O-…) or of type II (…-*A*O-$\mathbf{BO_2}$-$\mathbf{A'}$O-$B'O_2$-…); see Fig. 2. These last kinds of interfaces introduce the lowest atomic disorder and thus should be energetically favored. Obviously, steps of approximately 0.4 nm (one unit cell) height, or half-steps ($\sim$0.2 nm), corresponding to a mixed configuration of types I and type II, may occur at a real interface. In our case, the type-II configuration (…-$La_{2/3}Sr_{1/3}$O-$\mathbf{MnO_2}$-$\mathbf{SrO}$-TiO_2-…) induces a modification of the atomic neighboring of Mn cations. Considering the two neighboring planes of the MnO_2 interface plane, the La/Sr ratio locally changes from 2 (in bulk LSMO) to $\frac{1}{2}$ at the interface. In configuration I (…MnO_2-$\mathbf{La_{2/3}Sr_{1/3}O}$-$\mathbf{TiO_2}$-SrO-…) the last MnO_2 plane is covered by a $La_{2/3}Sr_{1/3}O$ plane, thus keeping the neighboring of the bulk material.[20,21]

We have tried to see if the HRTEM images allow us to decide between type-I and -II interface configurations. Thickness-defocus maps have been calculated for supercells modeling the two configurations. In Fig. 4, we show the simulation for a type-I configuration with an optimal contrast for a defocus value of -33 nm and a good match with the corresponding experimental images in the upper part of the figure. The interface, easily seen from the crossover from tiny $La_{2/3}Sr_{1/3}$ atomic columns (in LSMO) to strongly visible Sr atomic columns (in STO), is indicated by an arrow on both experimental and simulated images. However, the simulation for the type-II interface configuration (TiO_2 replaced by MnO_2 between $La_{2/3}Sr_{1/3}O$ and SrO) leads to similar simulated images and to a similar agreement with the experimental ones. The differences between the two set of simulated image being of the order of magnitude of the noise in

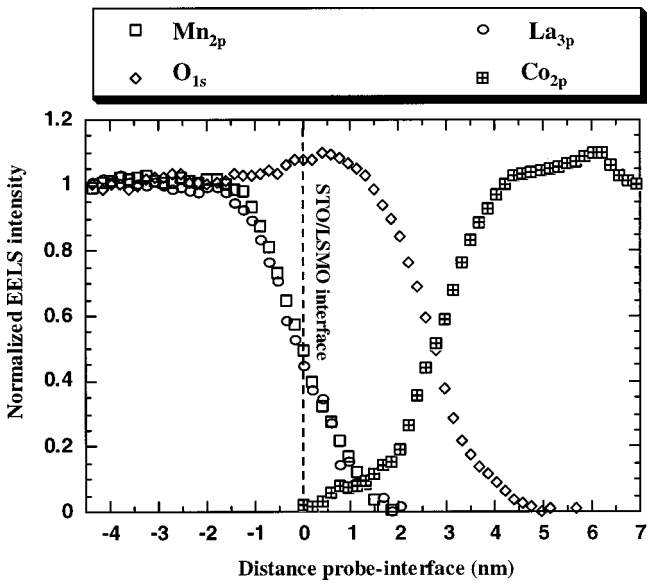

FIG. 5. Elemental profiles for the O_{1s}, Mn_{2p}, Co_{2p}, and La_{3d} edges acquired across the multilayers using the image spectrum technique. The beam size is 0.7 nm, the probe step 0.3 nm and the corresponding step for the distance probe interface is 0.2 nm. The intensity of the edges are normalized to the Mn_{2p} LSMO signal.

experimental pictures, we conclude that this simple comparison between simulated and experimental HRTEM image cannot allow us to distinguish between the type-I and II configurations. This analysis, however, confirms that the roughness of the interface is at the very most of one unit cell.[22]

B. Elemental profile and description of the Mn_{2p} and O_{1s} edges

The structural information obtained from the above HRTEM study (continuity of the lattice through the STO/LSMO interface, the abrupt interface up to one atomic plane, the stability of the lattice parameter, and the low specimen thickness variation) is very helpful for the spatially resolved chemical analysis. On the other hand, thanks to the reduced acquisition time available with our apparatus, our EELS study consists of recording several thousand spectra. The present results are thus representative of the material and do not only correspond to few spectra collected randomly.

1. Elemental profiles across the interface

Figure 5 exhibits EELS elemental profiles for O, Mn, Co, and La across the sequence of layers LSMO/STO/Co, extracted from a series of EELS spectra recorded in optimum conditions. The intensity decrease for Mn and La at the LSMO/STO interface is slightly softer than expected for a probe diameter of 0.7 nm, with the electron beam exactly parallel to the interface. This can be reasonably ascribed to some tilt (about 3°) between the beam direction and the interface plane, and is not indicative of any interface disorder. Otherwise, since the elemental composition is known in LSMO and STO layers, the experimental ratio of the inelastic scattering cross sections for the selected elements (La, Mn, O and Co) can be determined. The difference between these experimental values and the calculated ones using the Hartree-Slater method is less than 10%.[23] The oxygen intensity is slightly increased within the STO layer. This small variation can be due to slight specimen thickness changes induced by variable specimen thinning rate. However, it remains sufficiently low to be undetected from the HRTEM observations. An inelastic cross section variation between the O $1s$ edge in LSMO and STO could also explain this intensity increase.

A further information is the very good agreement between the Mn and La profiles. The relative proportion of these two atomic species is stable up to the interface. The position of the latter is taken at the half intensity of Mn or La signals.

2. Description of the ELNES structure for the Mn_{2p} and O_{1s} edges as a function of the Sr/La ratio

The valence properties of $La_{1-x}Sr_xMnO_3$ as a function of the Sr/La $(=x/1-x)$ ratio have up to now been studied mostly by means of x-ray-absorption spectroscopy (XAS) on bulk material.[24] Mn_{2p} and O_{1s} edges are the main relevant signals to characterize the changes in unoccupied electron states. They are also very well suited to EELS analysis, in which case these two edges can be collected in the same acquisition to avoid any instrumental problem. The first step is to relate the ELNES to the composition (x) in order to have reference edge shapes for interpreting in a following step the changes in edge shapes occurring when scanning the probe from one material to the other across the interface.

(a). Mn_{2p} Three Mn_{2p} spectra are displayed in the normal mode in Fig. 6(a), corresponding to the compositions $La_{0.1}Sr_{0.9}MnO_3$ (what we call SMO, with $x=0.9$), $La_{2/3}Sr_{1/3}MnO_3$ (LSMO, with $x=\frac{1}{3}$) and $LaMnO_3$ (LMO, with $x=0$). Note that the perovskite structure is maintained over the whole x range from 0 to 0.9. The hexagonal structure of the pure Mn^{4+} ($SrMnO_3$) phase is without interest for the present study. All the displayed spectra exhibit two ''white lines'' L_3 $(2p_{3/2})$ (642–643 eV) and L_2 $(2p_{1/2})$ (652.5–653 eV) dominated by strong multiplet effects due to Coulomb and exchange interactions between the $2p$ core hole and the $3d$ electrons in the final states. The peak shapes and chemical shifts are very sensitive to the $3d$ ground-state configuration as well as to the crystal-field interaction, and can be used to determine $3d$ occupancy and the valence states. Figure 6(a) shows that the $2p_{3/2}$ edge regularly shifts of about 1 eV toward higher-energy losses for increasing x values from 0 (LMO) to 0.9. This chemical shift is due to the change in the electrostatic energy at the Mn site induced by the decrease in the occupation of the $3d$ states. It can be used as a fingerprint to monitor the valence state across the LSMO layer up to the interface with the STO barrier. The LMO ($x=0$) spectrum is similar to the Mn_{2p} of Mn_2O_3 with Mn^{3+} in a slightly distorted octahedral symmetry[25] while the SMO spectrum is very close to the MnO_2 spectrum with Mn^{4+} in octahedral symmetry. Furthermore the splitting of the L_3 ''white line'' increases with the crystal-field strength [Fig. 6(a)]. For a high value of the crystal field ($10Dq=2.4$ eV) corresponding to the high Sr concentration, a weak sharper

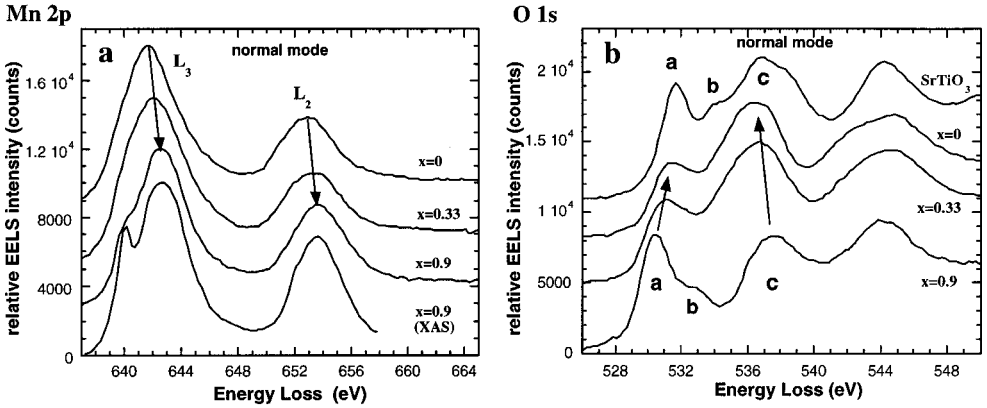

FIG. 6. (a) Mn_{2p} EELS reference spectra of $La_{(1-x)}Sr_{(x)}MnO_3$ for three x values. The arrows indicates the multiplet shifts. (b) O_{1s} EELS reference spectra of $La_{(1-x)}Sr_{(x)}MnO_3$ for three x values. $SrTiO_3$ is also shown. The arrows indicates the multiplet shifts in LSMO. For peak *a*, the crossover from LSMO to STO shifts the line to the higher energy, whereas the formation of $SrMnO_3$ (see the spectrum for $La_{0.1}Sr_{0.9}MnO_3$) should lead to a shift in the opposite direction. Conversely, the formation of $LaMnO_3$ does not lead to a significant shift of the peak.

peak appears at 640.8 eV clearly visible in XAS and convoluted in EELS by the lower instrumental energy resolution. Contrary to the L_3 transition, the L_2 structure is slightly broadened for the rich La composition.

(b). O_{1s} Contrary to the Mn case, the O_{1s} edge can be recorded on both sides of the LSMO/STO interface. Consequently spectra corresponding to LSMO with different x values as well as to STO are gathered in Fig. 6(b). O_{1s} spectra basically reflect the unoccupied oxygen p character. Intraatomic multiplet effects are negligible, and this kind of spectrum is usually interpreted on the basis of partial density-of-states calculations. The O_{2p} character is hybridized with $3d$ metal states, forming empty bands of predominantly metal weight above the Fermi level.[26] Both spectra exhibit the characteristic features of that of the perovskite structure. Structures '*a*' and '*b*' are respectively related to the e_g and t_{2g} states resulting from the splitting of the $3d$ band induced by the crystal field $(10Dq)$. These two structures have already been described for the MnO_2 and TiO_2 compounds which are of rutile structure also composed of MnO_6 or (TiO_6) octahedrons.[26,27] Moreover, the energy shifts of peaks '*a*' and '*b*,' between $SrTiO_3$ and $SrMnO_3$ $(x=0.9)$, are nearly the same as those already reported in Ref. 28 for the TiO_2 and MnO_2 oxides. When the Sr/La ratio is increasing, several changes appear. The intensity of the first peak at 531 eV (structure '*a*'), strongly increases, which reveals more visibly than on the corresponding Mn_{2p} edge, the change of Mn valence from 3 to 4 corresponding to a higher density of unoccupied *d* states above the Fermi level. Structure '*c*' can be attributed to the hybridization of the O_{2p} state with either the Sr_{4d} states (in the cases of $SrTiO_3$ and $SrMnO_3$) or the La_{5d} state (in the case of $LaMnO_3$).[24]

Considering peak '*a*,' the crossover from LSMO to STO shifts the line to higher energy, whereas the formation of $SrMnO_3$ should lead to a shift in the opposite direction. Conversely, the formation of $LaMnO_3$ does not lead to a significant shift of the line.

In conclusion, the situation for the O_{1s} edge is more complicated than for Mn_{2p} edge due to the presence of the additional STO signal. The spectra presented in second derivative mode helps to detect the different possibilities (Fig. 7). To get to the bottom of the ELNES description at the LSMO/STO interface, the presentation is broken into two parts: the eventual detection of an increase of Mn^{4+} character and the neighboring of the Mn atoms in the ultimate atomic planes.

C. Valence of the Mn at the interface?

First, Fig. 7 shows that the Mn_{2p} (a) and the O_{1s} (b) edges in the LSMO layer (top of Fig. 7) are quite equivalent to the corresponding ones acquired from a bulk specimen (bottom of Fig. 7). Since the probe is moving along the interface plane with an angle of 20° (Fig. 3), the distance between the probe and the interface is decreasing down by 0.2 nm for each probe step (see Sec. II B). Using the spectrum-image technique, the most representative spectra are displayed in Fig. 7. Focusing on the Mn spectra, we see that the EELS signal is decreasing to 0 at $+0.5$ nm (that is when the probe begins to be entirely within the STO barrier).

The main information which is revealed on these figures, is that for both Mn_{2p} and O_{1s} edges, there is no energy shift (or no ELNES deviation) indicating an increased proportion of Mn^{4+}. The large amount of spectra including the interface area with a large overlapping between each probe position ensure this result. The absence of a Mn^{4+} enhancement is mathematically confirmed, using a NNLS fit (not shown here) with adequate Mn_{2p} and O_{1s} reference spectra. The 'SMO' profile looks like a quite delocalized residual noise. Taking into account the beam size which covers about three atomic planes and the probe step (0.2 nm perpendicularly to the interface) as well as the result consistency for the Mn and O edges, the conclusion is that we do not detect any enhancement of Mn^{4+} character up to the last atomic plane in contact with the STO barrier.

We thus find that the stabilization of the effective interface T_c at about its bulk value is associated with the conservation of the bulk valence at the interface. In contrast, in the

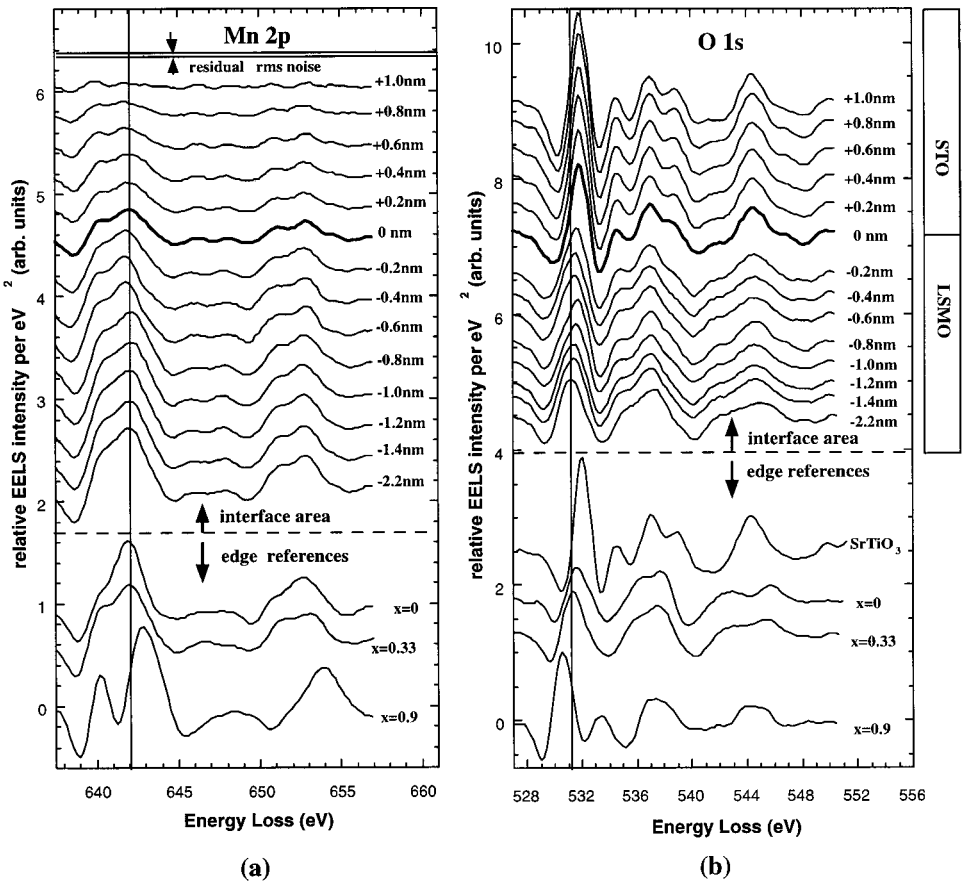

FIG. 7. (a) Evolution of the Mn-L edge across the LSMO/STO interface. A second energy derivative mode is used. The distance from the interface is displayed. The position "0 nm" corresponds to the interface position located from the Mn signal (Fig. 4). The corresponding reference spectra for three Sr concentrations are also displayed $(La_{(1-x)}Sr_x)MnO_3$. (b) Evolution of the O 1s edge across the LSMO/STO interface. The position "0 nm" corresponds to the interface position located from the Mn signal (Fig. 4). The corresponding reference spectra for three Sr concentrations $(La_{(1-x)}Sr_x)MnO_3$ and $SrTiO_3$ are displayed.

work of Bibes[9] on LCMO thin films, one finds a strong reduction of the magnetization that is associated with an increase of the relative weight of the Mn^{4+} line in the NMR spectrum of Mn.[55] This has been associated with an inhomogeneous state mixing metallic and insulating phases and a proportion of metallic phase vanishing for thin films. We point out that, although we have recorded several dozens of STEM-EELS scans at various places of the interface, we have not explored the entire interface and we cannot completely rule out the existence of very small and isolated areas with different phase. If such small areas with insulating phases exist, this would not affect the TMR and its temperature dependence as the tunneling current can only arise from the bulklike metallic part of the interface. Note, finally, that our results on the valence conservation are consistent with a termination of LSMO by $La_{2/3}Sr_{1/3}O$ (type I) without direct contact of the last MnO_2 layer with the first SrO layer of STO.

D. Neighboring of Mn at the interface

The last point is finding the origin of the enhancement of the shoulder on the left side of the Mn-L_3 line, with a more visible splitting of the two lines at the approach of the interface [Fig. 7(a)].

1. Interface signal extraction

Since Mn atoms are located only on one side of the interface, the EELS signal coming from the interface is highlighted when the probe is going past the apex of the interface and therefore mostly located in the STO barrier [Fig. 7(a)]. For this probe position, the limitation usually comes from the signal-noise ratio (SNR) because the signal is decreasing to zero. The interest of using MSA is first to increase the SNR. As any thresholding method, MSA must be used under specific conditions in order to valid the built up information. Without detailing the application of MSA, this signal analysis consists mainly in studying the intensity of the eigenvector modulus, the spatial location and the shape of the signal included in these vectors. MSA applied to the Mn_{2p} signal confirms the energy shift and the increasing of the splitting observed over the $Mn_{2p3/2}$ edge [Fig. 7(a)].

2. Discussion of the splitting of the Mn_{2p} edge at the interface

The splitting clearly visible on several spectra on the $Mn_{2p3/2}$ signal can be attributed either to an increase of the crystal field ($10Dq$) resulting from a slight compression of the MnO_6 octahedral cage or to a distortion of this octahedron compared to the bulk configuration. Plausible origins of the distortion might be a partial loss of oxygen in the last $La_{2/3}Sr_{1/3}O$ and MnO_2 layers at the interface, or/and in the epitaxial strain at the interface. This suggests an alternative scenario to the $La_{2/3}Sr_{1/3}O$ termination (type I) which was one of our conclusions of Sec. III C to explain that the Mn-L_3 line does not show a shift to highest energy. This alternative scenario would combine oxygen vacancies with a type II termination of LSMO, that is with the last MnO_2 layer between $La_{2/3}Sr_{1/3}O$ and SrO. Without oxygen vacan-

cies, this would lead to a shift toward highest energy (decrease of the Mn^{3+}/Mn^{4+} ratio) which is not seen in the Mn-L spectra. With oxygen vacancies, this shift to highest energy could be compensated for by an opposite shift due to the deficit of oxygen. However, quantitatively, this alternative scenario is hardly consistent with the experimental results: a straightforward calculation shows that, with a type-II termination, the valence of Mn in the last MnO_2 layer keep its bulk value with $O_{2.92\ (or\ less)}$ instead of O_3 in the manganite formula. According to what one knows on the influence of the oxygen vacancies of O,[29] this would lead to a dramatic decrease of the Curie temperature, that we do not find (this would also lead to a strong increase of the lattice parameter that we would have observed). Moreover, we do not observe any specific signal on the O_{1s} spectra when the probe is located near the interface; indeed, the shape of the O_{1s} edge continuously changes from LSMO to STO. In conclusion, the alternative scenario combining a type-II termination with a deficit of oxygen in the last LSMO layer would require too large a concentration of vacancies, and is hardly consistent with our data. The only realistic interpretation of our whole set of data is by a predominant proportion of type-I interface with LSMO terminated by a $La_{2/3}Sr_{1/3}O$ layer. A small deficit in oxygen probably explains the enhanced splitting at the approach of the interface. Theoretical simulations are needed for a more quantitative interpretation.

IV. CONCLUSION

The objective of the present work was to obtain a detailed characterization of the atomic scale structure at the STO/LSMO interface of Co/STO/LSMO tunnel junctions for which we had already investigated the tunnel magnetoresistance (TMR) properties. One knows that the TMR of tunnel junction is essentially determined by the spin polarization in the first atomic layers of the magnetic material at the barrier/electrode interface. For Co/STO/LSMO junctions presenting TMR effects practically up to T_c^{bulk}, we wanted to know the STO/LSMO interface structure at the origin of a much smaller reduction of the effective interface T_c (Ref. 5) than at other STO/LSMO interfaces (for example at the top interface of our LSMO/STO/LSMO junction).

Our HRTEM experiments show the quality of the pseudomorph growth of LSMO and STO (with the in-plane parameter of the STO substrate) and the continuity of the perovskite stacking sequence across the interface. They also confirm the abruptness of the STO/LSMO interface but does not allow us to determine whether the termination of LSMO is of type I (termination by a $La_{2/3}Sr_{1/3}O$ layer) or type II (termination by a MnO_2 layer).

However, our STEM-EELS data demonstrate that the valence of Mn keeps the value of bulk $La_{2/3}Sr_{1/3}MnO_3$, up to the last MnO_2 layer at the interface with STO (at least in a predominant proportion of the interface, as our scans have not explore the entire interface). There is no shift indicating an enhanced Mn^{4+} character. This certainly explains the very weak reduction of the interface T_c. To understand the structural properties accounting for the absence of shift to Mn^{4+} at the interface, we have considered two possible scenarii: (a) a predominant type-I termination with the last MnO_2 layer protected between two $La_{2/3}Sr_{1/3}O$ layers; and (b) a predominant type-II termination with the last MnO_2 layer between $La_{2/3}Sr_{1/3}O$ and SrO layers, but with a deficit in oxygen (consistent with a multiplet enhancement in the Mn-L EELS spectra when the electron probe is located at the interface cell of the LSMO structure) to compensate for the shift to Mn^{4+} induced by the proximity of the SrO layer. However, the required deficit of oxygen for the compensation was too large and inconsistent with our data.

We thus conclude that the conservation of the bulk valence of Mn in LSMO up to the last MnO_2 layer and the very weak reduction of T_c at the STO/LSMO interface of our Co/STO/LSMO junction are likely due to a predominant termination of LSMO by a $La_{2/3}Sr_{1/3}O$ layer at our ''bottom'' STO/LSMO interfaces. A similar study of a ''top'' LSMO/STO interface is in progress and should allow us to understand the difference in the termination or structure at the origin of the more strongly reduced T_c of LSMO/STO/LSMO tunnel junctions where both ''bottom'' and ''top'' LSMO/STO interfaces are involved.

ACKNOWLEDGMENTS

The authors are grateful to N. Bonnet and A. Gloter for helpful discussions about the MSA technique and multiplet effect, respectively. The authors are indebted to Marcel Tencé for the optimization of the experimental conditions using the EELS CCD camera. We also thank M. Bibes for useful discussion about phase segregation in manganite.

*Corresponding author. Email address: albert.fert@thalesgroup.com

[1] Y. Lu, X. W. Li, G. Q. Gong, Gang Xiao, A. Guptaz, P. Lecoeur, J. Z. Sun, Y. Y. Wang, and V. P. Dravid, Phys. Rev. B **54**, 8357 (1996).

[2] M. Viret, M. Drouet, J.-P. Contour, J. Nassar, C. Fermon, and A. Fert, Europhys. Lett. **39**, 545 (1997); J. Nassar, M. Viret, M. Drouet, J.-P. Contour, C. Fermon, and A. Fert, in *Science and Technology of Magnetic Oxides*, edited by M. Hundley, J. Nickel, R. Ramesh, and Y. Tokura, MRS Symposia Proceedings No. 494 (Materials Research Society, Pittsburgh, 1998), p. 231.

[3] J. S. Noh, T. K. Nath, C. B. Eom, J. Z. Sun, W. Tian, and X. Q. Pan, Appl. Phys. Lett. **79**, 233 (2001).

[4] Moon-Ho Jo, N. D. Mathur, N. K. Todd, and M. G. Blamire, Phys. Rev. B **61**, 14 905 (2000).

[5] The existence of an ''effective'' Curie temperature at an interface is not quite consistent with a single-phase picture of a ferromagnet. A more plausible picture is that with a phase inhomogeneity in the neighborhood of the interface with a collapse of the proportion of the bulklike ferromagnetic and metallic character at the ''effective'' Curie temperature of the interface. This type of picture has been described by Moon-Ho Jo *et al.* (Ref. 4).

[6] J.-M. De Teresa, A. Barthélémy, A. Fert, J.-P. Contour, R. Lyonnet, F. Montaigne, P. Seneor, and A. Vaures, Phys. Rev. Lett. **82**,

4288 (1999); Science **286**, 507 (1999).
[7] A. Fert *et al.* Mater. Sci. Eng., B **84**, 1 (2001).
[8] M. Izumi, Y. Konishi, T. Nishihara, S. Hayashi, M. Shinohara, M. Kawasaki, and Y. Tokura, Appl. Phys. Lett. **73**, 2497 (1998).
[9] M. Bibes, Ph.D. thesis, Institut National des sciences Appliquées de Toulouse and Universitat Autònoma de Barcelona.
[10] J. Ayache and P. H. Albarède, Ultramicroscopy **60**, 195 (1995).
[11] J. Benedict, R. Anderson, S. Klepeis, and M. Chaker, in *Specimen Preparation for Transmission Electron Microscopy of Materials II*, edited by R. Anderson, MRS Symposia Proceedings No. 199 (Materials Research Society, Pittsburgh, 1990), p. 189.
[12] P. Stadelman, Ultramicroscopy **21**, 131 (1987).
[13] Spectrometer modified at the ''Physique des Solides'' laboratory in Orsay by Marcel Tencé and Paul Ballongue (1999–2000).
[14] C. Jeanguillaume and C. Colliex, Ultramicroscopy **28**, 252 (1989).
[15] N. Bonnet, N. Brun, and C. Colliex, Ultramicroscopy **77**, 97 (1999).
[16] P. Trebbia and N. Bonnet, Ultramicroscopy **34**, 165 (1990).
[17] M. Tencé, M. Quartuccio, and C. Colliex, Ultramicroscopy **58**, 1 (1995); **58**, 42 (1995).
[18] V. E. Henrich and P. A. Cox, *The Surface Science of Metal Oxides* (Cambridge University Press, Cambridge, 1994).
[19] G. Koster, G. Rijnders, D. H. A. Blank, and H. Rogalla, Physica C **339**, 215 (2000).
[20] T. Suzuki, Y. Nishi, and M. Fujimoto, Philos. Mag. A **80**, 621 (2000).
[21] D. Fuchs, M. Adam, P. Schweiss, S. Gerhold, S. Schuppler, and R. Schneider, J. Appl. Phys. **88**, 1844 (2000).
[22] J.-L. Maurice, R. Lyonnet, and J.-P. Contour, J. Magn. Magn. Mater. **211**, 91 (2000).
[23] R. D. Leapman, P. Rez, and D. F. Mayers, J. Chem. Phys. **72**, 1232 (1980).
[24] M. Abbate, F. M. F. de Groot, J. C. Fuggle, A. Fujimori, O. Strebel, F. Lopez, M. Domke, G. Kaindl, G. A. Sawatzky, M. Takano, Y. Takeda, H. Eisaki, and S. Uchida, Phys. Rev. B **46**, 4511 (1992).
[25] H. Paterson and O. L. Krivanek, Ultramicroscopy **32**, 313 (1990).
[26] M. Grioni, M. T. Czyzyk, F. M. F. de Groot, J. C. Fuggle, and B. E. Watts, Phys. Rev. B **39**, 4886 (1990).
[27] H. Kurata, E. Lefevre, C. Colliex, and R. Brydson, Phys. Rev. B **47**, 13 763 (1993).
[28] H. Kurata and C. Colliex, Phys. Rev. B **48**, 2102 (1993).
[29] A. M. De Leon-Guevara, P. Berthet, J. Berthon, F. Millot, A. Revcolevschi, A. Anane, C. Dupas, K. Le Dang, J. P. Renard, and P. Veillet, Phys. Rev. B **56**, 6031 (1997).